

# 1 **Cost-optimal design of reverse electrodialysis process for** 2 **salinity gradient-based electricity in desalination plants**

3 *Energy*

4 C. Tristán<sup>a,\*</sup>, M. Fallanza<sup>a</sup>, I. Ortiz<sup>a</sup>, R. Ibáñez<sup>a</sup>, I. E. Grossmann<sup>b</sup>

5 <sup>a</sup> Department of Chemical and Biomolecular Engineering, University of Cantabria,  
6 Av. Los Castros 46, 39005 Santander, Spain.

7 <sup>b</sup> Department of Chemical Engineering, Carnegie Mellon University, Pittsburgh, PA 15213, USA

8 \*Corresponding author: [tristanc@unican.es](mailto:tristanc@unican.es)

## 9 **Abstract**

10 This work provides the cost-optimal design of a large-scale reverse electrodialysis (RED)  
11 system deployed in a medium-capacity desalination plant using mathematical  
12 programming. The optimization model determines the hydraulic topology and working  
13 conditions of the RED units that maximize the net present value (NPV) of the RED  
14 process. We examine how past and future trends in electricity and carbon prices,  
15 membranes price, desalination plant capacity, and the use of high-conductive membranes  
16 may affect the competitiveness and performance of the NPV-optimal design. We also  
17 compare the conventional series-parallel configuration, and the NPV-optimal solution  
18 with recycling and added reuse alternatives of the RED units' exhausted streams to size  
19 the benefits of mathematical programming over conventional heuristics. It is shown that  
20 in the context of soaring electricity prices and strong green financing support, with the  
21 use of high-performing, affordable membranes ( $\sim 10$  €/m<sup>2</sup>), RED could save 8% of  
22 desalination plant energy demand from the grid, earning profits of up to 5 million euros  
23 and LCOE of 66–126 €/MWh, which is comparable to other renewable and conventional  
24 power technologies. In such conditions, the optimization model finds profitable designs  
25 for the entire range of medium-capacity desalination plants, providing energy and  
26 emission savings from the grid.

- 27 **Keywords:** Renewable energy; Generalized Disjunctive Programming; Desalination;
- 28 Wastewater reuse; Water-energy nexus.

## 29 **1 Introduction**

30 The energy released by mixing two water streams of different salinities, so-called salinity  
31 gradient energy (SGE), is a vast yet largely untapped renewable power source [1,2] to  
32 complement and diversify the current carbon and water-intensive energy mix [3,4], and  
33 sustain the energy-intensive water sector [5]. SGE technologies offer an integrated  
34 approach to the United Nations' Sustainable Development Goal (SDG) 7 on affordable,  
35 reliable, sustainable energy access, and SDG 6 on clean water and sanitation.

36 Desalination and wastewater reuse are projected to increase in the coming decades [6,7]  
37 to reduce withdrawals from conventional surface and groundwater resources, while  
38 meeting stringent water quality standards. However, as large energy users of conventional  
39 power sources [8,9], they are also large greenhouse gas (GHG) emitters that question their  
40 sustainability [10–12]. Seawater reverse osmosis (SWRO), the technology of choice in  
41 the global desalination market [13,14], is getting closer to the practical minimum energy  
42 to desalinate seawater hitting a record, low specific energy consumption (SEC) of  
43  $\sim 2$  kWh/m<sup>3</sup> of desalted water [8]. Despite the marked decline in SEC, the carbon footprint  
44 of large-scale desalination plants remains an issue [15,16]. Hence, coupling desalination  
45 with renewable energy sources will be vital for the sustainable production of desalinated  
46 water [12,17]. SGE technologies can provide clean, base-load electricity to desalination  
47 and wastewater treatment plants, supporting their decarbonization and circularity [5].

48 Within the SGE technologies, reverse electrodialysis (RED) has made great progress in  
49 the past two decades, and is now closer to commercialization with some pilot trials and  
50 field demonstrations [18–24]. In principle, a RED system takes in low- and high-salinity  
51 waters (LC and HC) on either side of alternate pairs of cation-exchange (CEM) and  
52 anion-exchange (AEM) membranes that let through counter-ions, but not co-ions and  
53 water [25]. The salinity difference over each ion-exchange membrane (IEM) creates an

54 electrochemical potential that drives the diffusion of cations through CEMs towards the  
55 cathode, and anions through AEMs towards the anode from the saltier stream to the  
56 less-salty side; redox reactions at the outer electrodes convert this ionic flow into an  
57 electron flux. The electric potential of the membrane pile and the resulting electric current  
58 can then be used to power the external load.

59 The low power density of large-scale RED (0.38–2.7 W/m<sup>2</sup> total membrane area), fouling,  
60 and high cost of commercial membranes are the main limitations for RED technological  
61 readiness [1,26,27]. Niche markets beyond utility-scale electricity open new avenues to  
62 prove and advance RED market readiness. For instance, seawater desalination brine and  
63 wastewater are discarded streams that can be exploited to produce and save energy while  
64 minimizing the environmental impact of brine disposal [28]. Besides, desalination’s  
65 seawater influent is already pre-treated to remove foulants [29], so the rejected brine  
66 would likely be less prone to cause fouling than raw seawater, which would require  
67 further energy-intensive purification.

68 While several studies have investigated the design of the RED process to improve the  
69 power density and/or the energy conversion efficiency (i.e., the fraction of SGE converted  
70 into useful work) of single [30–34] or several RED units in series or simple layouts, few  
71 have considered more complex topologies—which may yield optimal designs—and cost  
72 metrics (e.g., net present value, levelized cost of electricity), which are key drivers for  
73 widespread RED adoption [35–38]. Efficiency and power density are mutually exclusive  
74 performance metrics as maximizing both requires differing operating conditions [39].  
75 Multi-staging of the RED stacks and electrode segmentation can provide efficient designs  
76 with higher power densities than once-through RED operation with unsegmented  
77 electrodes [40]. Multi-staging adds more degrees of freedom to the design and operation  
78 space, such as individual electrical control of the stages [41–43] like electrode

79 segmentation [44–47], asymmetric staging (i.e., different spacer thickness, number of cell  
80 pairs, membrane properties, path length and type of mixing promoters in each stage)  
81 [40,48,49], and different configurations [43,47,50,51]. However, these studies do not  
82 consider the cost, which is a key enabler of RED technology adoption.

83 An alternative to making decisions about RED process design is to use  
84 optimization-based methods that rigorously search for the optimal configuration in a  
85 given design space [52,53]. Notably, Generalized Disjunctive Programming (GDP) is a  
86 higher-level modeling framework that makes the formulation process more intuitive and  
87 systematic, while preserving the underlying logic structure of the problem in the model  
88 [54]. Tristán et al. [55] developed a GDP optimization model that incorporates a detailed  
89 model of the RED stack [56,57] to define the hydraulic topology and the working  
90 conditions of a set of RED units that maximize the net present value (NPV) of the RED  
91 process. Their work illustrates the functionality and benefits of mathematical  
92 programming and GDP modeling on the conceptual design and optimization of the RED  
93 process over conventional heuristics.

94 This follow-up study applies the GDP optimization model [55] to define the cost-optimal  
95 design of a large-scale RED system in a medium-capacity SWRO desalination plant, a  
96 favorable market to prove and advance RED-based electricity. The assessment explores  
97 how electricity and emissions allowances prices over time, membranes price, SWRO  
98 desalination plant capacity, and membranes resistance, may affect the cost-optimal  
99 design, economic feasibility, and competitiveness of the RED process. To evaluate the  
100 benefits of the GDP model over heuristics, we also compare the conventional  
101 series-parallel configuration with the optimal solution to the GDP problem, which  
102 includes recycling and reuse alternatives of the exhausted streams of the RED units. This  
103 case study serves to gauge the emissions and energy savings from the water- and

104 carbon-intensive grid mix the RED system can offer to desalination in the most  
105 cost-conscious way, the way forward to make RED-based electricity a full-scale reality.

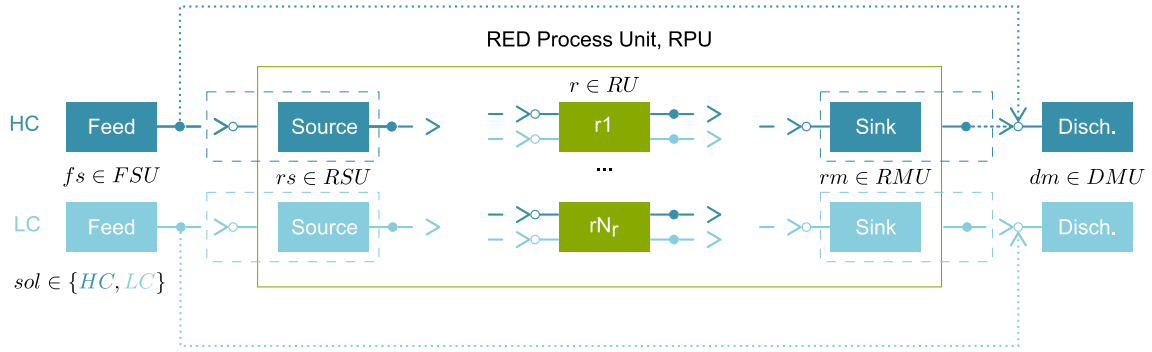
## 106 **2 Methods**

107 Optimization-based strategies involve three major steps: (i) postulating a superstructure  
108 that embeds the relevant flowsheet alternatives from which the optimum solution is  
109 selected, (ii) its formulation as a tractable mathematical programming model; and  
110 (iii) solving the model with an optimization algorithm to determine the optimal  
111 configuration [52,58]. Since the GDP model for the optimal design of the RED process  
112 is thoroughly described in [55], we will brief the reader on the main equations and  
113 assumptions.

### 114 **2.1 Problem statement and superstructure definition**

115 The problem addressed is to determine the hydraulic topology, that is, the number and  
116 hydraulic arrangement of the RED units and their working conditions (e.g., electric  
117 current, inlet flow velocities, and molar concentrations) that yield the cost-optimal  
118 flowsheet design of the RED process for a given concentration, volume, and temperature  
119 of the high-salinity and low-salinity feed streams, and a fixed design of the RED stacks.

120 The superstructure in Fig. 1 displays the feasible design alternatives for the stated  
121 problem, i.e., RED-based electricity production from the embedded energy of the HC and  
122 LC feed waste streams, with  $N_r$  conditional RED units. The reader is referred to [55] for  
123 details on the superstructure definition and notation.



124

125 **Fig. 1.** Superstructure for the RED process. High (HC) and low-salinity (LC) feed ( $fs \in FSU$ ) and discharge ( $dm \in DMU$ ) units. The set of source ( $rs \in RSU$ ) and sink ( $rm \in RMU$ ) units and the set of candidate RED units ( $r \in RU$ ) are children of the parent RED Process unit (RPU).

## 129 2.2 Optimization model

130 The set of equations (1) describes the general form of the Generalized Disjunctive  
 131 Programming (GDP) optimization model for the superstructure in Fig. 1. GDP models  
 132 involve continuous and Boolean variables with constraints in the form of algebraic  
 133 expressions, conditional constraints within disjunctions, and logical propositions. The  $Nr$   
 134 two-term disjunctions represent the discrete activation and deactivation of the  $Nr$   
 135 candidate RED units.

$$\begin{aligned}
 \max NPV &= f(x) \\
 \text{s. t. } &g(x) \leq 0 \\
 &\left[ \begin{array}{c} Y_r \\ h_r(x) \leq 0 \end{array} \right] \vee \left[ \begin{array}{c} \neg Y_r \\ B^r x = 0 \end{array} \right] \quad \forall r \in RU \\
 &\Omega(Y_r) = True \\
 &x \in X \subseteq R^n \\
 &Y_r = \{True, False\} \quad \forall r \in RU
 \end{aligned} \tag{1}$$

137 In problem (1), the objective is to maximize the Net Present Value (NPV) of the RED  
 138 process subject to inequality constraints from process specifications and equality  
 139 constraints from material, energy balances, and thermodynamic relationships. The  
 140 continuous variables  $x$  are the molar concentrations and volumetric flows of the streams,  
 141 and the internal variables of the active RED units. Decisions are made on the electric  
 142 current and the concentration and flowrate of the RED stack's inlet streams. The global

143 constraints,  $g(x) \leq 0$ , outside the disjunctions are equalities and inequalities describing  
144 specifications and physical relationships that apply for all feasible configurations in the  
145 superstructure, e.g., mass balances of the feed, source, sink, and discharge units, and the  
146 upper and lower bounds on concentration and flowrate. In each term of the disjunctions,  
147 the Boolean variables  $Y_r$  define the existence or absence of the RED unit; if a unit exists  
148 or is selected ( $Y_r = True$ ), the associated active constraints  $h_r(x) \leq 0$  impose the  
149 relevant mass and energy balances or other physicochemical phenomena that apply in the  
150 RED unit, add the incurred capital and operating cost to the objective function, and set  
151 lower and upper bounds on its internal variables and the concentration and flowrate of its  
152 inlet and outlet streams; otherwise, the negation ( $\neg Y_r$ ) ignores the RED unit equations in  
153 the inactive disjunctive term, and  $B^r x = 0$  constraints set to zero a subset of the  
154 continuous variables and cost terms in the objective function. Other types of logical  
155 relationships for selecting the candidate RED units ( $\Omega(Y_r) = True$ ) are specified using  
156 logic propositions.

157 To formulate the GDP problem, we assume:

- 158 (a) The feed streams are pure sodium chloride (NaCl) solutions, thus neglecting the  
159 non-idealities of aqueous solution (i.e., unity activity coefficients) and the existence  
160 of other species that would undermine the RED performance.
- 161 (b) The internal losses depend only on the ionic resistance of solutions and membranes.
- 162 (c) Constant membranes permselectivity and ionic resistance apply, regardless of the  
163 solutions concentration and temperature.
- 164 (d) There is no water transport across the membranes against the concentration gradient  
165 due to osmosis, which implies a constant streamwise volumetric flowrate in RED's  
166 channel.



- 167 (e) Salt diffusivities in the membrane phase are independent of solutions concentration  
 168 and temperature.
- 169 (f) No fluid leakage or ionic shortcut currents in the RED stack's manifolds.
- 170 (g) Co-current flow of the high- and low-concentration streams.
- 171 (h) The RED system operates under isothermal and isobaric conditions.

172 The solution to the GDP model maximizes the NPV of the RED process (2), which  
 173 considers operating (OPEX in €/year), and capital costs (CAPEX in €) annualized over  
 174 the expected lifetime of the plant  $LT$  in years, using the capital recovery factor,  $CRF$ ,  
 175 given in (4) with a discount rate  $DR$ . The OPEX and annualized CAPEX define the total  
 176 annual cost (3),  $TAC$ , of the RED system. The NPV accounts for electricity sales and  
 177 carbon pricing revenues. The RED plant electricity is sold to the grid at Spanish average  
 178 price of electricity for non-house consumers,  $ep$  [59], and the abated GHG emissions  
 179 from the grid mix (Spanish emission factor,  $ef$ ) are subsidized at the average price,  $cp$ ,  
 180 in the European Union Emission Trading System (EU ETS) [60].

$$181 \quad NPV = \frac{(ep + cp ef) TNP - TAC}{CRF} \quad (2)$$

$$182 \quad TAC = CRF CAPEX + OPEX \quad (3)$$

$$183 \quad CRF = \frac{DR}{1 - (1 + DR)^{-LT}} \quad (4)$$

$$184 \quad TNP = \sum_{r \in RU} NP_r \quad (5)$$

185 We use a semi-rigorous version of Tristán et al. [55,56] RED stack model, to balance  
 186 model fidelity and tractability. When the RED unit is active ( $Y_r = \text{True}$ ), the discretized  
 187 model predicts the net power output,  $NP_r$ , that is added to the net power capacity of the

188 RED system, i.e., total net power,  $TNP$  in kW (5). When the RED unit is absent ( $\neg Y_r$ ) the  
 189 net power output is set to zero.

190 We consider plant downtime due to membrane cleaning and system maintenance by  
 191 applying a load factor,  $LF$ , to the annual energy yield (kWh/year) of the RED plant  
 192 working at full capacity.

193 To estimate the capital investment, we determine the cost of RED stacks,  $\sum_{r \in RU} CC_{stack,r}$ ,  
 194 pumps,  $CC_{pump}$ , and civil and electrical infrastructure costs,  $CC_{civil}$ .

$$195 \quad CAPEX = \sum_{r \in RU} CC_{stack,r} + CC_{pump} + CC_{civil} \quad (6)$$

196 The annual operating cost comprises the electricity cost from pumps,  $\sum_{r \in RU} OC_{pump,r}$ ,  
 197 the replacement cost of membranes,  $\sum_{r \in RU} OC_{IEMSrep,r}$ , and maintenance and labor costs.

$$198 \quad OPEX = \sum_{r \in RU} OC_{pump,r} + \sum_{r \in RU} OC_{IEMSrep,r} + 0.02 CAPEX \quad (7)$$

199 When the RED unit is active,  $CC_{stack,r}$  is added to CAPEX, and  $OC_{pump,r}$  and  $OC_{IEMSrep}$   
 200 to OPEX; otherwise, these terms take zero values.

201 The objective function in (2) is maximized subject to constraints in the GDP that are  
 202 detailed in Tristán et al. [55]. The remainder financial parameters are those reported in  
 203 Table 1.

204 **Table 1.** Financial parameters for the RED plant.

Parameter	Value
Plant lifetime, $LT$ (years)	30
Membranes' lifetime, $LT_m$ (years)	10
Load Factor, $LF$	90%
Discount rate, $DR$	5%
Spanish emission factor, $ef$ (kg CO <sub>2</sub> -eq/kWh)	0.374

205

### 206 **2.3 Solution strategy**

207 We code the GDP model using the Python-based, algebraic modeling language Pyomo  
208 [61] and Pyomo.GDP, a Pyomo library extension for logic-based modeling and  
209 optimization [62]. To solve the GDP problem, we apply the Global Logic-based Outer  
210 Approximation (GLOA) algorithm [63,64] implemented in the logic-based solver  
211 GDPopt version 20.2.28 built on Pyomo.GDP. The GLOA algorithm decomposes the  
212 solution to the GDP into a sequence of mixed-integer linear programming (MILP) master  
213 problems and reduced nonlinear programming (NLP) subproblems.

214 We solve the MILP master problems with CPLEX and the NLP subproblems with the  
215 multistart heuristic algorithm MSNLP using IPOPTH as a local NLP solver on a machine  
216 running Windows 10 (x64) with 6 cores processor (Intel® Core™ i7-8700 CPU  
217 @3.2 GHz) and 16 GB of RAM. We access the MINLP and NLP solvers from GAMS  
218 34.1.0 through the Pyomo-GAMS interface. The stopping criteria depend upon the  
219 specified MSNLP solver's maximum number of iterations to guarantee a near-optimal  
220 solution.

### 221 **2.4 Techno-economic performance metrics**

222 To assess the technical performance of the optimal RED process designs, we determine  
223 its net power density, i.e., the net power produced per membrane area, and its net energy  
224 efficiency, or the fraction of exergy or theoretical maximum energy attainable in form of  
225 SG, converted to useful work. We consider the Levelized Cost of Energy (LCOE) to  
226 assess the cost-competitiveness of the RED optimal designs.

#### 227 **Net and thermodynamic energy efficiency**

228 The exergy or Gibbs free energy of mixing is the theoretical maximum energy that is  
229 available for useful work from a system reaching equilibrium. The difference in the Gibbs

230 free energy between the final mixture and the initial high and low-salinity solutions yields  
 231 the change in free energy of mixing of the inlet  $\Delta G_{mix,in}$  and outlet  $\Delta G_{mix,out}$  (8) streams  
 232 of the RED process unit, i.e. streams  $(fso, rsu)$  and  $(rmu, dmi)$  [44,65].

$$233 \quad \Delta G_{mix,i} = 2 R T \sum_{sol \in \{HC, LC\}} Q_{i,sol} C_{i,sol} \ln \frac{C_{i,sol}}{C_{M,i}} \quad (8)$$

$$\forall i \in in \cup out = (fso, rsu) \cup (rmu, dmi)$$

$$234 \quad C_{M,i} = \frac{\sum_{sol \in \{HC, LC\}} Q_{i,sol} C_{i,sol}}{\sum_{sol \in \{HC, LC\}} Q_{i,sol}} \quad (9)$$

$$\forall i \in in \cup out = (fso, rsu) \cup (rmu, dmi)$$

235 where  $R$  is the gas constant (8.314 J/mol/K),  $T$  is the absolute temperature (K), 2 denotes  
 236 the number of ions each NaCl molecule dissociates into,  $Q$  is the volumetric flowrate  
 237 ( $m^3/s$ ) and  $C$  the concentration ( $mol/m^3$ ) of the initial high and low-salinity solutions  
 238 entering and leaving the RED process. Equation (9) yields the concentration of the mixed  
 239 solution in thermodynamic equilibrium ( $C_M$  in  $mol/m^3$ ) of the RED process inflow and  
 240 outflow streams.

241 The net energy efficiency,  $\eta_{net}$ , measures the input fraction of free energy that RED  
 242 converts into electricity (10). The exergy change between RED process inlet and outlet  
 243 streams is the exergy recovered for conversion, i.e., the retrieved exergy for useful work  
 244 ( $\Delta G_{mix,retrieved}$ ), that is used to compute the thermodynamic efficiency,  $\eta_{th}$ , of the RED  
 245 process.

$$246 \quad \eta_{net} = \frac{TNP}{\Delta G_{mix,in}} \quad (10)$$

$$247 \quad \eta_{th} = \frac{TNP}{\Delta G_{mix,in} - \Delta G_{mix,out}} = \frac{TNP}{\Delta G_{mix,retrieved}} \quad (11)$$

## 248 **Levelized Cost of Energy (LCOE)**

249 The LCOE (€/kWh) estimates the average cost per unit of energy generated during the  
250 lifetime of a power plant that would break even the RED project costs. The LCOE gives  
251 a first-order assessment of the RED project viability. Assuming the energy provided  
252 annually is constant during the lifetime of the project, the LCOE reduces to (12).

$$253 \quad LCOE = \frac{CRF CAPEX + OPEX}{TNP 8760 LF} - cp \quad ef \quad (12)$$

## 254 **2.5 Specifications for the RED optimal design deployed in a medium-size** 255 **desalination plant**

256 The large-scale RED system recovers energy from the concentrate effluent of  
257 Maspalomas II SWRO desalination plant in Gran Canaria (Canary Islands, Spain) [66–  
258 68]. Maspalomas II plant produces 26,184 m<sup>3</sup>/day of desalted water and rejects  
259 17,602 m<sup>3</sup>/day of high-salinity brine (1.67 M NaCl, 20 °C) with a SEC of 3.77 kWh/m<sup>3</sup>.  
260 The low-salinity feedwater (20mM NaCl) may be obtained from nearby wastewater  
261 treatment plants (e.g., el Tablero, las Burras) [69]. Hence, we assume the same LC and  
262 HC feed volume available for SGE conversion.

263 The case study explores how (i) electricity and carbon prices, (ii) membrane price,  
264 (iii) desalination plant capacity, and (iv) membrane resistance, may affect the  
265 cost-competitiveness, power density, and energy efficiency of the NPV-optimal RED  
266 design. All the assessments refer to a commercial RED unit (Table 2) in 2022, unless  
267 otherwise stated.

268 **Table 2.** Parameters of the commercial RED stack (Fumatech GmbH<sup>®</sup>, Germany).

<b>Parameter</b>	<b>Value</b>
Number of cell pairs	1000
Channel size	1.824 m × 1.532 m <sup>a</sup>
<b>Spacers</b>	
Thickness (μm)	270 <sup>b</sup>
Porosity	82.5%
<b>Membranes properties: fumasep<sup>®</sup> CEM (FKS-50) / AEM (FAS-50)</b>	
Areal resistance (Ω·cm <sup>2</sup> )	1.8 / 0.6 <sup>c</sup> (-20%) <sup>d</sup>
Permselectivity (-)	0.93
Thickness dry (μm)	50
Active area (m <sup>2</sup> )	0.7 <sup>a</sup>

269 <sup>a</sup> Four times the size of fumatech<sup>®</sup> ED-1750 pilot-scale module. <sup>b</sup> Equal to  
 270 inter-membrane distance, i.e., HC or the LC channels height. <sup>c</sup> Measured in 0.5 M NaCl  
 271 at 25 °C. <sup>d</sup> Reduction assuming future advances in membranes design.

272 To assess the influence of electricity price and carbon pricing over time, we gather  
 273 Spanish average electricity price [59] and EU ETS average emission allowances price  
 274 [60] for the period 2017–2022. We regress EU-27 data from 2007 onwards [59] to  
 275 estimate 2030 electricity prices; the carbon price in 2030 is a central estimate benchmark  
 276 from OECD [70]. We assess the sensitivity to membrane costs by setting values between  
 277 the current price of membranes (i.e., average CEM and AEM cost from Fumatech<sup>®</sup>, 87.5  
 278 €/m<sup>2</sup>) and the lowest price reported in the literature (~10 €/m<sup>2</sup>) [71]. We assume 20%  
 279 drop in membranes resistance to reflect future advancements in membranes design. We  
 280 reduce the flowrate of both HC and LC feedwaters to estimate the minimum SWRO  
 281 desalination plant capacity that would allow the NPV-optimal RED process earn profits.

282 To evaluate the benefits of the GDP optimization model in RED process design over  
 283 heuristic approaches, we compare two hydraulic arrangements each with the same  
 284 number of candidate RED units (i.e.,  $N_r = 35$ ):

285 (i) Fixed series-parallel layout, from our previous assessment [56], where the RED  
 286 system treats desalination concentrate into several identical parallel arrays of units in  
 287 series, so neither recycling nor alternative reuse of the outlet streams is allowed. The

288 objective is to maximize the total net power of the parallel branch, as it was set in our  
289 previous study [56].

290 (ii) GDP layout, leaving the connection between the superstructure units free as a discrete  
291 decision. In this case, the objective is to maximize the NPV.

292 In the Series layout, we estimate the working conditions that maximize the net power of  
293 a stand-alone RED stack to fix the flowrate of the inlet streams to each parallel branch.  
294 We assume that the high and low salinity feedwaters are evenly split among the parallel  
295 branches, each with the same optimal configuration, so the net power output and costs of  
296 the RED system scale accordingly.

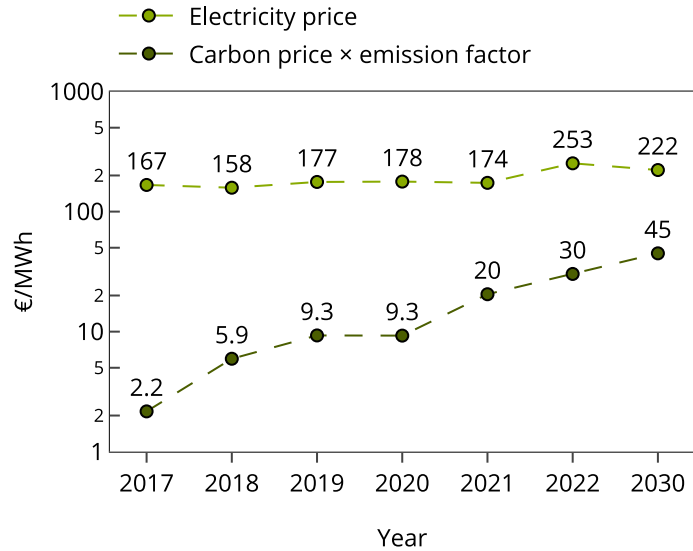
### 297 **3 Results and discussion**

298 For all the scenarios and the given parameters, each solution provides the NPV-optimal  
299 topology and decision variables that balance electricity production and capital and  
300 operating outlays increase. Discrete decisions include the working RED units and the  
301 active water streams. Continuous decisions are the flowrate and concentration of the inlet  
302 streams and the electric current of each active RED stack.

303 It is worth noting that simplifications and assumptions of the RED stack model [55] result  
304 in an overestimation of the net power output and, as such, an underestimation of the  
305 LCOE and an overestimation of the NPV.

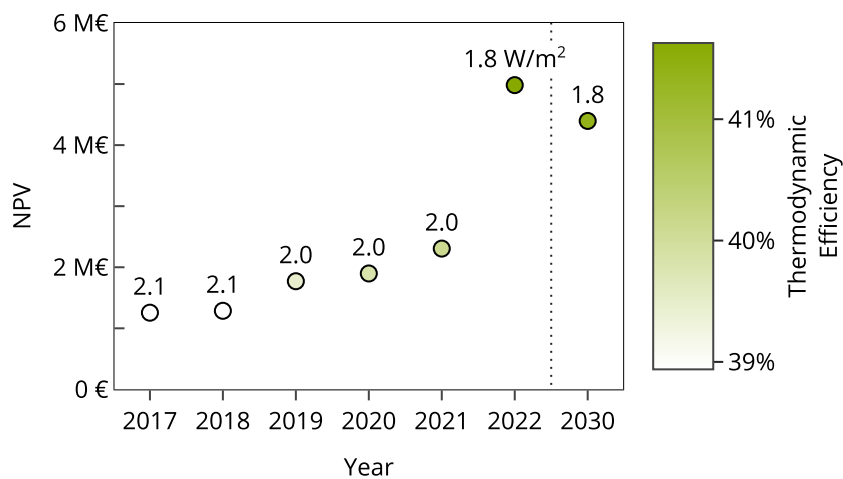
#### 306 **3.1 Electricity and carbon price assessment**

307 As expected, the upward trend of electricity and emissions allowances prices over time  
308 (Fig. 2) favors RED process techno-economic performance (Fig. 3), which in turn relieves  
309 the grid mix supply of Maspalomas II desalination plant (RED-based electricity could  
310 meet about ~7–8% of the SEC).



311

312 **Fig. 2.** Revenues per MWh from electricity and emission allowances over the period  
 313 2017–2022 with projections to 2030



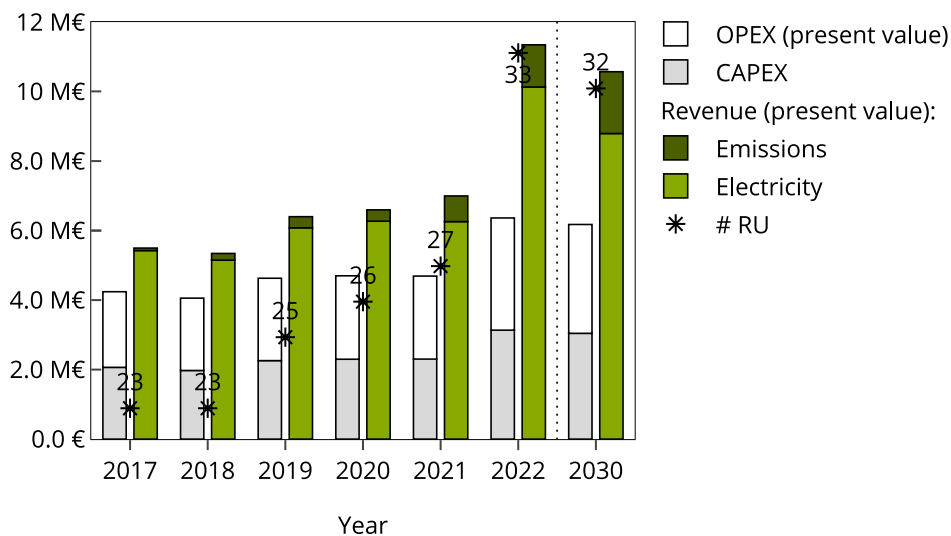
314

315 **Fig. 3.** Net present value, net power density (markers text), and thermodynamic energy  
 316 efficiency (markers color) of the NPV-optimal RED process design over the past five  
 317 years from 2022 and forecast to 2030.

318 Russia’s invasion of Ukraine in early 2022 brought severe disruptions in the EU energy  
 319 market. The unprecedented surge in European fossil gas prices is echoed in the unparallel  
 320 electricity price spike in 2022 (Fig. 2), soaring prices that incentivizes the promotion of  
 321 emerging renewable technologies such as RED. Besides, the cap-and-trade EU ETS limits  
 322 the volume of allowances in the market over time (Fig. 2) to comply with emissions  
 323 reduction targets, the scarcity of emission allowances (among other factors) increases  
 324 their price used in financing RED (Fig. 4).



325 For the assessed period (Fig. 4), electricity sales are the main source of revenue, with  
 326 lower yet growing revenue shares from auctioning allowances in the EU ETS (e.g., from  
 327 1% of all revenues in 2017 to ~11% in 2022 and ~17% in 2030). As a result, RED benefits  
 328 grow by about 52% in five years, a 25% increase in NPV. Despite the slight decline of  
 329 electricity price in 2030, the RED process may raise 724,155 euros each year during their  
 330 lifetime yielding a NPV of about 4.4 million euros.



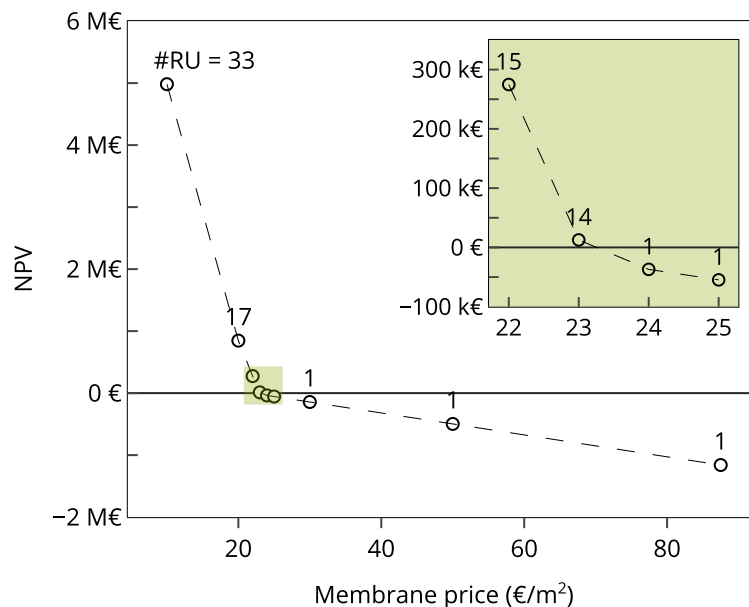
331  
 332 **Fig. 4.** NPV-optimal RED process over the period 2017–2022 with projections to 2030:  
 333 cost and revenues breakdown in present value and number of active RED units, # RU.  
 334 When electricity is priced high, the revenue gained outstrips the increase in costs from a  
 335 larger number of RED units (Fig. 4). The optimal solution therefore activates more RED  
 336 units to raise the nominal generation capacity of the RED system (10 units in five years  
 337 delivering 23% more TNP), but at a cost. Each unit added to the RED system reduces the  
 338 overall net power density from 2.1 W/m<sup>2</sup> in 2017 to 1.8 W/m<sup>2</sup> in 2022 (Fig. 3). On the  
 339 flip side, the RED system retrieves more exergy for conversion (15% more exergy than  
 340 in 2017) from which a greater share (39% in 2017 and 42% in 2022) is converted into net  
 341 electricity, enhancing the overall energy efficiency and net power output of the RED  
 342 system (Fig. 3).

343 The overall net power density loss is related to the lower inlet flowrate of the RED units.  
 344 This is because the same HC and LC feed volumes (kept constant throughout the years)  
 345 are sourced to a larger number of RED units. Such lower inlet flowrate causes the RED  
 346 units to depart from the net-power optimal working conditions, thereby reducing its  
 347 power rate.

348 These findings indicate that in a context of high electricity prices and strong green  
 349 financial support, RED technology does not require to reach the ambitious  $\sim 2.0 \text{ W/m}^2$  to  
 350 be competitive as previous studies suggested. This is a reassuring result for RED  
 351 transition from lab-scale to commercialization.

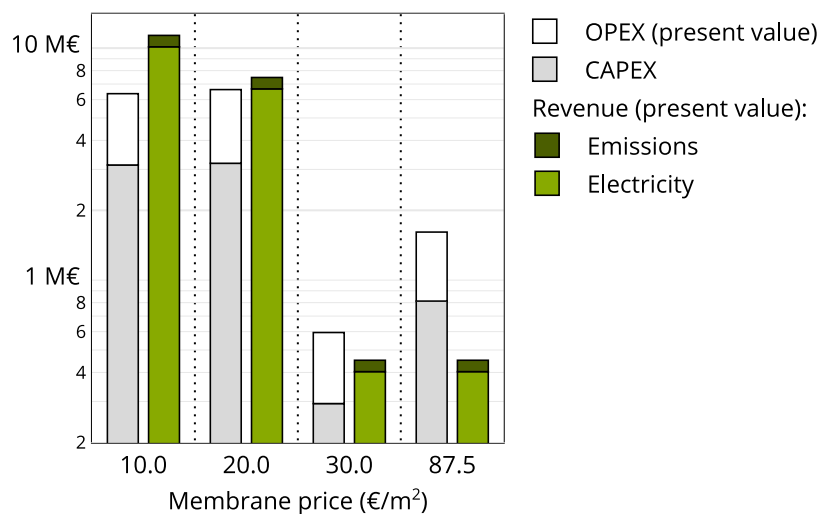
### 352 3.2 Membrane price assessment

353 The membrane price that breaks even the NPV-optimal RED design falls somewhere  
 354 between  $23 \text{ €/m}^2$  and  $24 \text{ €/m}^2$  (Fig. 5), just under twice to six times the price of previous  
 355 estimates of similar feeds concentrations (see Table 3).



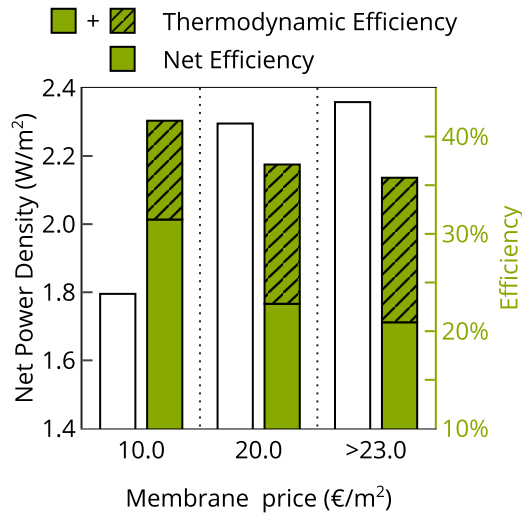
356  
 357 **Fig. 5.** Membrane price influence on the NPV-optimal RED process design: net present  
 358 value and number of active RED units. The inset magnifies the NPV in the membrane  
 359 price range within the boxed part of the graph.

360 Membranes priced above 23 €/m<sup>2</sup> yield larger economic losses when more than one RED  
 361 unit is active, that is, the capital and operational expenses overshadow incomes from  
 362 electricity sales and green financing incentives to a greater extent with an increasing  
 363 number of working RED units (Fig. 6); therefore, the optimal RED process design keeps  
 364 one RED unit active under near-optimal working conditions (i.e., maximum net  
 365 generation), which results in a higher power density of 2.4 W/m<sup>2</sup> but reduced net (21%)  
 366 and thermodynamic (36%) efficiencies (Fig. 7). As a result, the net power output and the  
 367 derived electricity and emissions revenues from a single RED unit remain unchanged,  
 368 whereas the investment and operational costs (i.e., membranes' replacement cost)  
 369 increase linearly with membrane price (Fig. 6). The balance between the constant  
 370 revenues and higher total costs of a single but costlier RED stack is reflected in the linear  
 371 decline of NPV with membrane price (Fig. 5).



372

373 **Fig. 6.** Membrane price influence on the NPV-optimal RED process design: cost and  
 374 revenues breakdown in present values.



375

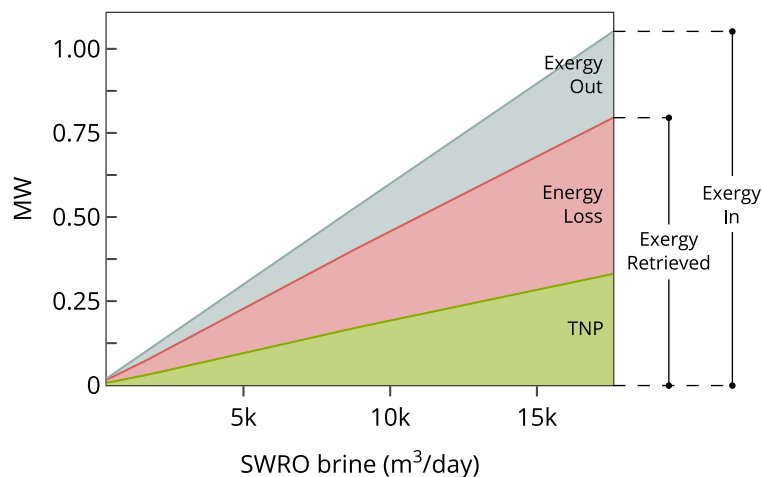
376 **Fig. 7.** Membrane price influence on the NPV-optimal RED process design: net power  
 377 density, net and thermodynamic energy efficiencies.

378 The NPV trend shifts for membranes rated below 23 €/m<sup>2</sup>, following a steep increase with  
 379 lower membrane prices (Fig. 5). As membrane price falls the GDP model activates more  
 380 RED units since the revenues earned outweigh the increase in capital and operating cost.  
 381 The overall net power density decreases due to the larger number of RED units fed with  
 382 the same feed flowrate, which recover a larger fraction of the input exergy for conversion  
 383 increasing the net efficiency (Fig. 7). The thermodynamic efficiency also increases  
 384 because the active RED units operate at lower inlet flowrates, reducing the overall pump  
 385 power consumption.

386 With the reduction of membrane costs, designers can focus on achieving higher energy  
 387 recovery rates from SG, leading to the development of more efficient and economically  
 388 viable designs that increase the RED-based share of the SWRO desalination plant supply  
 389 from 0.3% from a single costlier RED unit to 8% from 33 cheaper RED units. The  
 390 scale-up of the RED process capacity to the MW order would likely make the project  
 391 profitable in the short run if cheaper manufacturing membrane processes lower its cost to  
 392 ~20 €/m<sup>2</sup>.

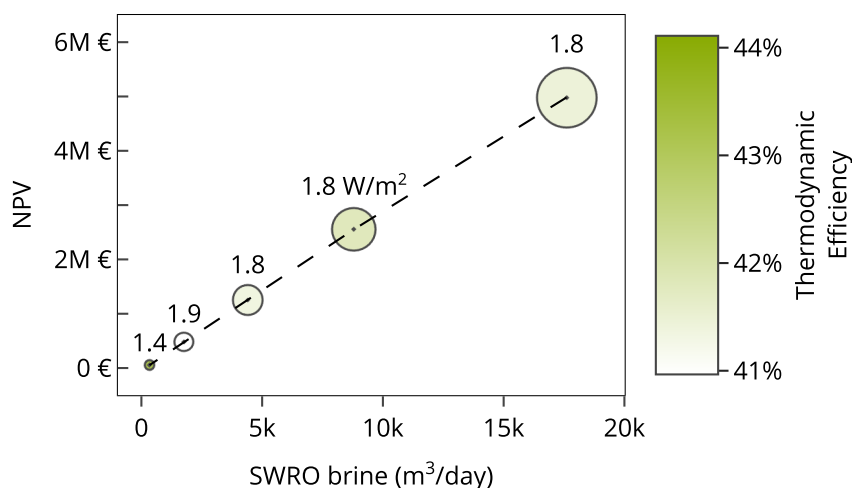
393 **3.3 SWRO desalination plant capacity assessment**

394 The available feeds flowrate restricts the exergy input which in turn bounds the useful  
395 work of the RED process. The exergy input scales linearly with the desalination plant  
396 capacity (Fig. 8), and so does the TNP of the RED plant (Fig. 8 and markers size in Fig.  
397 9). As such, to maximize the NPV with scarce feed volumes, the GDP optimization model  
398 deactivates RED units (keeping a single RED unit in the low-end capacity range of  
399 medium-sized SWRO desalination plants, i.e., 500 m<sup>3</sup>/day). By reducing the number of  
400 RED units, the NPV-optimal RED process attempts to emulate the overall working  
401 conditions with larger feed volumes. With larger HC and LC feed volumes (4400–  
402 17,600 m<sup>3</sup>/day) the NPV-optimal solution retrieves ~76% and converts ~31% of the input  
403 exergy into electricity (TNP) (Fig. 8). The net power density and thermodynamic  
404 efficiency (Fig. 9) remain roughly constant at ~1.8 W/m<sup>2</sup> and ~42% up to a tenth of  
405 Maspalomas II capacity. owing to the lower number of RED units (3 units) operating with  
406 larger, net-power optimal flowrates that increase the net power density to 1.9 W/m<sup>2</sup> with  
407 a slight decline in thermodynamic efficiency (41%).



408

409 **Fig. 8.** SWRO desalination plant capacity influence on the NPV-optimal RED process  
410 design: energy balance.



411

412 **Fig. 9.** SWRO desalination plant capacity influence on the NPV-optimal RED process  
 413 design: net present value, net power density (markers text), total net power output  
 414 (markers size), and net thermodynamic efficiency (markers color).

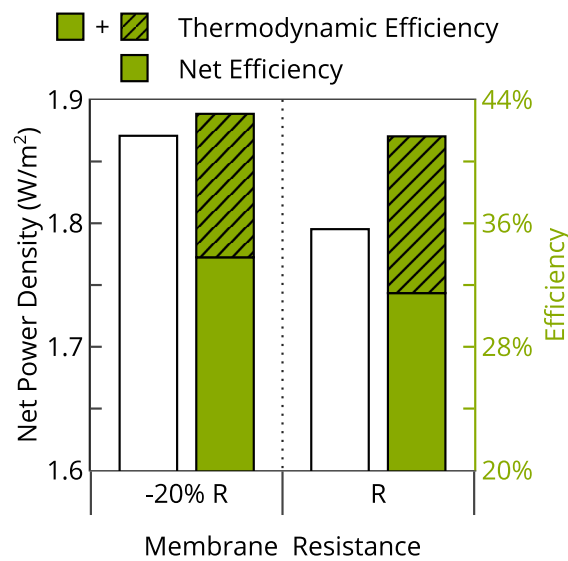
415 Desalination plants rejecting  $\sim 334$  m<sup>3</sup>/day (i.e., 500 m<sup>3</sup>/day nominal capacity), would  
 416 allow to install a single RED unit, that must run with a lower sub-optimal flowrate due to  
 417 the scarce HC and LC feed flowrates, as such the net power density decreases to  
 418 1.4 W/m<sup>2</sup>, while the energy efficiency increases to 44% (Fig. 9). This is because the RED  
 419 unit depletes to a greater extent the concentration gradient with lower hydrodynamic  
 420 losses. Even so, the RED unit would source about 7.5 kW to the desalination plant with  
 421 a profit of 53,595 euros.

422 Overall, the integration of on-site electricity generation based on RED technology in  
 423 desalination plants of up to 500 m<sup>3</sup>/day capacity can alleviate the reliance on water and  
 424 energy-intensive grid mixes, contributing to more sustainable and self-sufficient water  
 425 supply systems.

### 426 3.4 Membrane resistance assessment

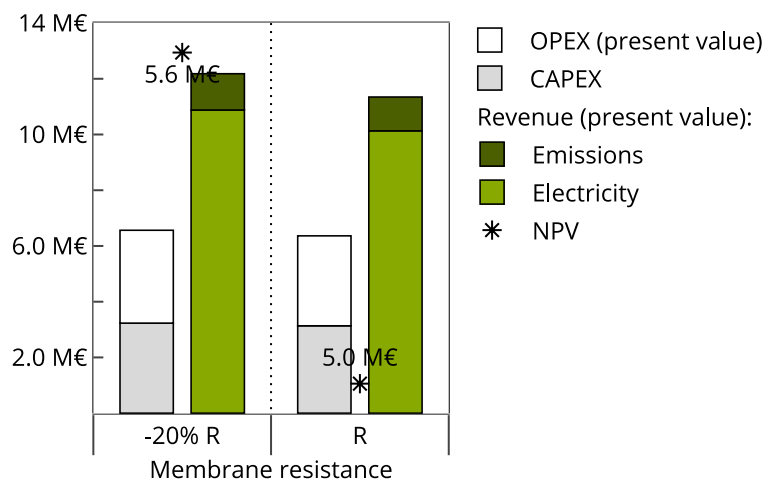
427 The use of high-performance membranes would provide slightly more powerful—i.e.,  
 428 7.4% more TNP with a 4.2% increase in the overall net power density (Fig. 10)—and  
 429 efficient designs—3.5% more efficient in terms of thermodynamic efficiency (Fig.  
 430 10)—by simply adding a RED unit to the RED system (about 5.6 km<sup>2</sup> of total IEM area

431 in a single stack). Such a small improvement would add up almost a million euros of  
 432 benefits with virtually no impact on capital and operational costs, resulting in a 13% NPV  
 433 increase (Fig. 11). The LCOE would also improve, moving from 103 €/MWh to  
 434 97 €/MWh. These results emphasize that any improvement in membranes' performance  
 435 has a positive impact on cost-competitiveness and widespread adoption of RED, a solid  
 436 reason to thrust the development of cost-effective manufacturing processes and mass  
 437 production of low-resistance membranes to reach prices of ~10 €/m<sup>2</sup>.



438

439 **Fig. 10.** Membrane resistance influence on the net power density, net and thermodynamic  
 440 energy efficiencies of the NPV-optimal design.



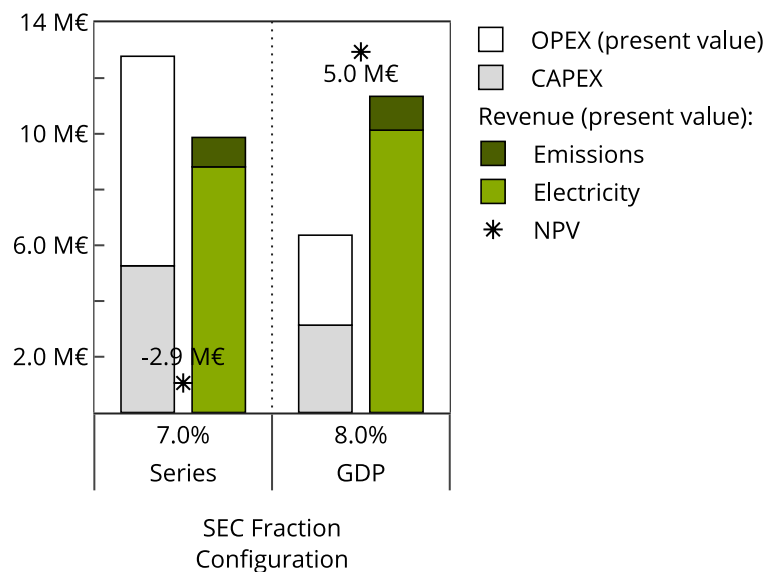
441

442 **Fig. 11.** Membrane resistance influence on the NPV-optimal design: cost and revenues  
 443 breakdown in present values and net present value (markers).

444 **3.5 Conventional series-parallel layout vs. NPV-optimal layout**

445 The optimal GDP layout outperforms the series-parallel arrangement, as it renders  
 446 economically viable RED process designs with almost equal energy and emissions  
 447 savings from the grid (~7% in the conventional layout and ~8% in the cost-optimal  
 448 layout).

449 The optimal series-parallel design of the RED process that peaks the total net power  
 450 output with (i) a fixed hydraulic arrangement of the RED units, (ii) fixed concentration  
 451 and flowrate of the HC and LC inlet water streams, and (iii) leaving the number of  
 452 working RED units and its electric current as single decision variables, is far from being  
 453 profitable (negative NPV of 2.9 million euros, Fig. 12). The GDP optimization model  
 454 activates the largest feasible number of RED units in series, i.e., 5 out of the 35 candidate  
 455 RED units per parallel branch, to maximize the net power generation of the whole system.  
 456 Even though the last RED units in the series increase the net power of the system, the  
 457 RED unit's net power density well decreases from the first 1.9 W/m<sup>2</sup> to the last  
 458 ~7 mW/m<sup>2</sup>, which makes them prohibitively expensive.

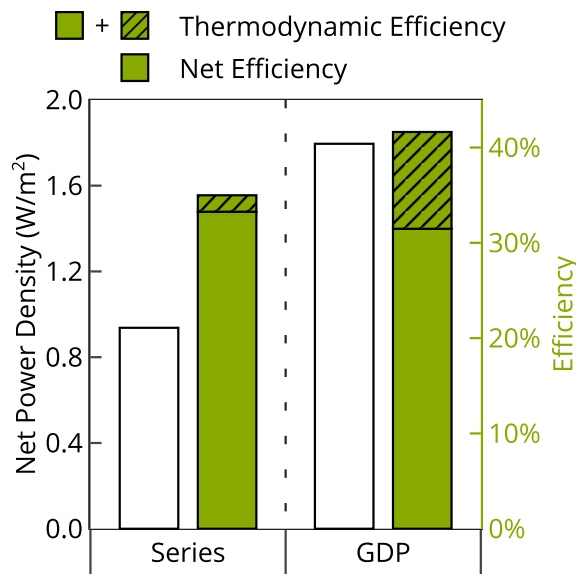


459  
 460 **Fig. 12.** Cost and revenues breakdown in present value and net present value of the  
 461 series-parallel and NPV-optimal layouts.



462 While the net energy efficiency of the series layout (33%, Fig. 13) aligns with the  
 463 estimated value to make RED technology competitive with other renewables (i.e., 40%)  
 464 [20], the total net power density (0.9 W/m<sup>2</sup>, Fig. 13) falls well below the estimated value  
 465 to make RED cost-competitive (2.0 W/m<sup>2</sup>) [20]. The capital and operational expenses  
 466 outweigh the benefits from electricity sales and green financing incentives which cover  
 467 78% of the total costs, as seen in Fig. 12.

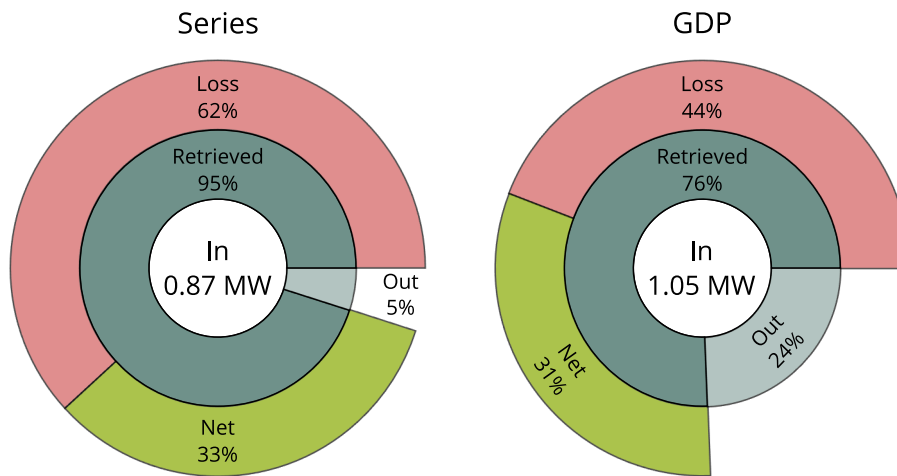
468 These results show that the optimal design from the technical perspective is not always  
 469 the same from an economical viewpoint. The series configuration recovers a larger  
 470 fraction of SGE at expense of lower power density that renders the RED process  
 471 unprofitable.



472  
 473 **Fig. 13.** Overall net power density, thermodynamic efficiency, and net energy efficiency  
 474 of the series-parallel and NPV-optimal layouts.

475 Even though the conventional layout retrieves more energy for conversion (by increasing  
 476 the extent of mixing through the series), the input exergy is lower than the optimal GDP  
 477 layout (Fig. 14). This is because the total LC feed (assumed equal to Maspalomas II's  
 478 desalination brine, ~733 m<sup>3</sup>/h) restricts the number of parallel branches to 11. The optimal  
 479 net-power inlet flowrate is about 0.6 times lower than the inlet LC flowrate. As such,

480 around 42% of the brine remains untapped reducing the input exergy of the RED system  
 481 to 866 kW (Fig. 14).



482  
 483 **Fig. 14.** Energy balance of the series-parallel and NPV-optimal layouts. In: Gibbs free  
 484 energy entering the RED system. Out: Gibbs free energy leaving the RED system unused.  
 485 Retrieved: Difference between input and output Gibbs free energies used for conversion  
 486 in the RED system. Loss: Gibbs free energy lost in energy conversion. Net: total net  
 487 power output of the RED system.

488 As opposed to the series arrangement, the GDP layout, with its (i) larger volume of HC  
 489 and LC feeds, and (ii) recycling and additional reuse alternatives, provides cost-optimal  
 490 designs that can earn large profits (Fig. 12) while reconciling high efficiency and higher  
 491 power densities (Fig. 13). The reduced extent of mixing and lower pump consumption of  
 492 the GDP layout (Fig. 14) improves the thermodynamic energy efficiency which increases  
 493 from 35% in the series-parallel arrangement to 42% in the GDP layout (Fig. 13) despite  
 494 the larger fraction of exergy unused (Fig. 14), which yields a modest decrease in net  
 495 efficiency (Fig. 13).

496 In the series-parallel arrangement, we enforce all RED units to work with higher flow  
 497 velocities, those that peak the net power of the stand-alone RED unit (2.6 cm/s in the HC  
 498 and 4.5 cm/s in the LC compartments). The effect of such high velocities is twofold: an  
 499 overall pump power increase (eight times the GDP's), which in turn raises the investment

500 and running costs (Fig. 12) and lowers the energy conversion efficiency (Loss in Fig. 14,  
501 and thermodynamic efficiency in Fig. 13).

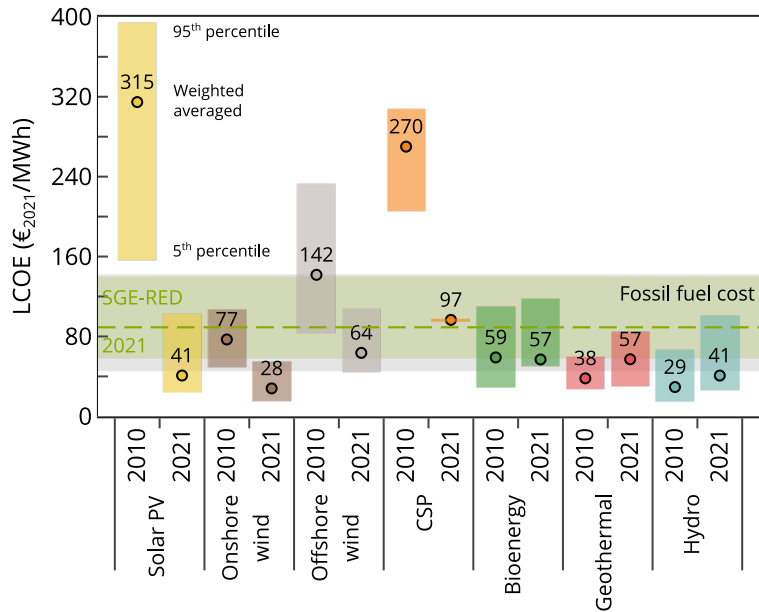
502 These results underscore the value of mathematical programming and higher-level GDP  
503 modeling over heuristics for determining cost-optimal RED flowsheet designs.

### 504 **3.6 Contextualizing RED economic competitiveness**

505 Despite the discrepancy between the assumptions and scale of renewables projects (i.e.,  
506 utility-scale projects of at least 1 MW) in IRENA's LCOE estimates [72] and the  
507 NPV-optimal LCOE of RED, Fig. 15 provides some insights into RED competitiveness.

508 The assumed low membrane cost of 10 €/m<sup>2</sup> in all the assessed years would make the  
509 LCOE of the NPV-optimal RED design fall within the range of fossil fuel-fired power  
510 generation technologies (Fig. 15). In the face of soaring electricity prices and stiff  
511 emission reduction targets to be on track of 2030 Paris Agreement's goals, the  
512 NPV-optimal RED process would even be on par (i.e., concentrated solar power, CSP) or  
513 in the range of other renewables.

514 If similar trends of steep cost reduction, technological advancements, and high  
515 penetration rates were to occur in RED technology, it is plausible that the LCOE for RED  
516 could reach levels comparable to established renewable technologies such as solar  
517 photovoltaic (PV) or onshore and offshore wind. This is in line with the steep cost  
518 reductions witnessed in solar PV, CSP, and offshore wind over the past decade (Fig. 15).  
519 Even though IRENA's analysis excludes the impact of government incentives or  
520 subsidies, carbon emission pricing or the benefits of renewables in reducing other  
521 externalities, these figures highlight the need to prove and advance RED to reach market  
522 readiness.



523

524 **Fig. 15.** Global LCOE from newly commissioned, utility-scale renewable power  
 525 generation technologies, 2010-2020 [72]. NPV-optimal RED process LCOE range  
 526 2017–2022 and 2030 (green filled area) and 2021 LCOE (green dashed line). Grey filled  
 527 area denotes price range of fossil fuel-fired technologies. All monetary values are in real,  
 528 2021 euros considering inflation and applying the exchange rate for each year.  
 529 PV: photovoltaic; CSP: concentrating solar power.

530 Table 3 compares reported cost estimates of RED and the LCOE of the NPV-optimal  
 531 RED process designs for current and future membrane price scenarios in 2022. The lack  
 532 of detailed economic evaluations and wide variability in LCOE (16–4956 €/MWh) across  
 533 existing studies due to disparity in their underlying financial and process assumptions,  
 534 makes any comparison inconclusive and open to discussion. As such, it serves to extract  
 535 some general guidelines and trends.

536 The HC and LC feed concentration, volume, and temperature determine the input exergy  
 537 and, thus, the nominal capacity and cost of the RED process. HC sources such as brines  
 538 from coal mines, desalination, saltworks, salt lakes, or regenerated thermolytic salt  
 539 solutions used in the so-called RED heat engines (1–5 M), offer higher SGE potential  
 540 than less salty water bodies such as seawater (0.5–0.6 M). A purposely designed RED  
 541 system could efficiently exploit these high-salinity sources, thus, reducing the LCOE.

542 Depending on the source, the feeds purity may also affect the performance and durability  
543 of RED if not properly pre-treated, which may increase capital and operational expenses.  
544 In this work, the objective function, i.e., the NPV, excludes the pre-treatment cost, which  
545 is likely to result in an underestimation of the actual LCOE for RED systems that use  
546 sources with extensive pre-treatment requirements, e.g., treated wastewater effluents, raw  
547 seawater, or river water.

548 None of the reported cost estimates in Table 3 consider the working conditions of each  
549 RED stack and their relative arrangement that may greatly improve both the performance  
550 and cost of the RED process as seen in the case study. Instead, most of them derived the  
551 cost of RED electricity or the LCOE for an estimated or projected RED unit power density  
552 or a targeted nominal capacity of the RED plant. Some also considered the impact of  
553 availability, concentration, and fouling potential of the HC and LC feeds, different RED  
554 stack sizes, and IEMs properties on RED system costs under fixed, suboptimal working  
555 conditions of the RED units. Such detailed assessments, however, miss cost-optimal  
556 design alternatives that optimization-based approaches can effectively handle and  
557 identify.

558 The case study and the reviewed studies reveal that realizing high-performing (i.e.,  
559 low-resistant, high-permeable), affordable membranes is a crucial lever for RED  
560 techno-economic progress toward market competitiveness. As shown in the case study,  
561 membrane cost weighs heavily on the objective function. Even though all scenarios have  
562 equal feedstreams conditions and candidate RED units, the high price of commercial  
563 membranes makes the NPV-optimal design uneconomic. Only if IEMs were  
564 one-order-of-magnitude cheaper, such that revenues offset the outlays increase, the  
565 NPV-optimal design would retain more RED units tuning their working conditions such  
566 that they reach the net power density that maximizes the NPV. The cumulative experience

567 in operating and developing RED technology will likely decrease its LCOE to the  
568 estimated 66–126 €/MWh.

**Table 3** Cost estimates of RED reported in the literature and the present study. TP: Total power. PD: Power density. DR: Discount rate.

	High-salinity solution	Low-salinity solution	TP (MW)	PD (W/m <sup>2</sup> )	Capacity Factor	Lifetime [years]		IEMs Price (€/m <sup>2</sup> ) <sup>f</sup>	DR	LCOE (€/MWh) <sup>f</sup>
						Plant	IEMs			
Turek (2007) [73]	0.6 M	9.6 mM	NR	0.46 <sup>a</sup>	NR	NR	10	73 (\$100/m <sup>2</sup> ) <sup>c</sup>	NR	4956 (6790) <sup>e</sup>
Turek (2008) [74]	1.9 M	9.6 mM	NR	1.04 <sup>a</sup>	NR	NR	10	68 (\$100/m <sup>2</sup> ) <sup>d</sup>	NR	2041 (3000) <sup>e</sup>
Post et al. (2010) [20]	0.5 M	5 mM	0.2	2 <sup>a</sup>	91%	20	7	2 10	6%	79 200
Daniilidis et al. (2014) [38]	0.5 M	17 mM	200	2.2 <sup>b</sup> 2.7 <sup>b</sup>	84%	25	7	4.3, 50 4	10%	18, 71 16
Weiner et al. (2015) [75]	0.6 M	17 mM	NR	1.2 <sup>b</sup>	NR	20	NR	676 (\$750/m <sup>2</sup> ) <sup>c</sup>	6%	5705 (6330)
Bevacqua et al. (2017) <sup>g</sup> [76]	2.6 M NH <sub>4</sub> HCO <sub>3</sub> 2.4 M NH <sub>4</sub> HCO <sub>3</sub> 2.5 M NH <sub>4</sub> HCO <sub>3</sub>	75 mM NH <sub>4</sub> HCO <sub>3</sub> 10 mM NH <sub>4</sub> HCO <sub>3</sub> 40 mM NH <sub>4</sub> HCO <sub>3</sub>	0.1 <sup>a</sup>	4.30 2.39 4.06	91%	20	NR	50	6%	683 306 436
Micari et al. (2019) <sup>g</sup> [77]	5 M	10 mM	1 <sup>b</sup>	3.2	90%	30	10	30	5%	400
Papapetrou et al. (2019) <sup>g</sup> [36]	3.8 M 5 M	10 mM 10 mM	0.1 1	0.66 <sup>b</sup> 4.67 <sup>b</sup>	90%	30	10	30	5%	1360 210
Giacalone et al. (2019) [37]	1.2 M 5 M	17 mM < 103 mM	2 <sup>b</sup> 4 <sup>b</sup> 0.01–1 <sup>b</sup> 0.04–3 <sup>b</sup>	1 <sup>a</sup> 2 <sup>a</sup> 1.5–2 <sup>a</sup> 6.5 <sup>a</sup>	90%	30	10	15 4, 15 15 4	5%	500 110, 250 270–330 30–50
Ranade et al. (2022) [78]	5 M	0.5 M	0.015 0.031	1.19 <sup>b</sup> 2.44 <sup>b</sup>	82%	20	10	5, 50	5%	250, 1500 120,750
This work <sup>h</sup>	1.67 M	20 mM	0.327 0.013	1.8 <sup>b</sup> 2.3 <sup>b</sup>	90%	30	10	10 87.5	5%	98 998

570 <sup>a</sup> Gross power. <sup>b</sup> Net power. <sup>c</sup> Total investment cost. <sup>d</sup> Including endplates and electrodes. <sup>e</sup> Cost of electricity. <sup>f</sup> Values between brackets in US \$ converted to € with the  
571 corresponding year average exchange ratio from the International Monetary Fund. <sup>g</sup> RED heat engine. <sup>h</sup> Circa 2022.



## 572 4 Conclusions

573 RED technology has great potential in solving the water-energy challenge but needs to  
574 prove that it can generate electricity reliably to gain the trust of investors and  
575 manufacturers to unlock economies-of-scale cost reduction. In this work, we have  
576 presented an optimization model to devise techno-economic viable RED process designs  
577 that support the leap from lab to market. The Generalized Disjunctive Programming  
578 (GDP) model allowed us to define the hydraulic topology and working conditions of a set  
579 of RED units to maximize the net present value of the RED process deployed in a  
580 medium-capacity seawater reverse osmosis plant.

581 We have estimated the energy and emissions savings from the grid RED-based electricity  
582 may offer to desalination exploring relevant factors involved in the cost-optimal design  
583 of the RED process, providing valuable insights:

584 (a) The growing electricity and emission allowance prices over time strengthen RED  
585 market readiness in niche applications such as desalination and wastewater treatment  
586 sectors, reaching LCOE of 66–126 €/MWh on par or in the range of other renewable  
587 and conventional power technologies.

588 (b) A realistic near-term reduction in membrane cost ( $\sim 20$  €/m<sup>2</sup>) would make RED  
589 profitable.

590 (c) The NPV-optimal RED process design may reap profits in medium-capacity SWRO  
591 desalination plants of up to 500 m<sup>3</sup>/day.

592 (d) The use of low-resistance, low-cost membranes does improve the  
593 cost-competitiveness of the RED process; a 20% drop in membranes resistance would  
594 increase profits by 13%.

595 (e) Recycling and reusing alternatives brings on RED process designs that attain profits,  
596 reduce grid mix emissions, and accommodate higher power densities and energy

597 efficiencies. Indeed, with a slightly lower RED-based take of the total desalination  
598 energy demand (~7% and ~8% in the series-parallel and NPV-optimal layouts), the  
599 series-parallel layout is as efficient as the GDP layout at the expense of a significant  
600 drop in power density which bears large economic losses.

601 These assessments show that mathematical programming is an efficient and systematic  
602 modeling and optimization tool to assist early-stage research, and to identify optimal  
603 design and operation guidelines for full-scale RED implementation. A natural progression  
604 of this work is to incorporate in decision-making uncertainty from electricity and  
605 emission allowances prices and membrane cost through stochastic optimization [79] and  
606 sustainability criteria through multi-objective optimization coupled with life cycle  
607 assessment principles [53].

608 **CReditTe authorship contribution statement**

609 **Carolina Tristán:** Conceptualization, Methodology, Software, Validation, Formal  
610 analysis, Investigation, Data curation, Writing - Original Draft, Visualization. **Marcos**  
611 **Fallanza:** Conceptualization, Writing - Review & Editing, Supervision. **Raquel Ibáñez:**  
612 Conceptualization, Resources, Writing - Review & Editing, Supervision, Project  
613 administration, Funding acquisition. **Inmaculada Ortiz:** Resources, Funding acquisition.  
614 **Ignacio E. Grossmann:** Conceptualization, Methodology, Resources, Writing - Review  
615 & Editing, Supervision

616 **Acknowledgments**

617 This work was supported by the LIFE Programme of the European Union (LIFE19  
618 ENV/ES/000143); the MCIN/AEI/10.13039/501100011033 and “European Union  
619 NextGenerationEU/PRTR” (PDC2021-120786-I00); and by the  
620 MCIN/AEI/10.13039/501100011033 and “ESF Investing in your future” (PRE2018-  
621 086454)

622 **References**

- 623 [1] Tufa RA, Pawlowski S, Veerman J, Bouzek K, Fontananova E, di Profio G, et al.  
624 Progress and prospects in reverse electro dialysis for salinity gradient energy  
625 conversion and storage. *Appl Energy* 2018;225:290–331.  
626 <https://doi.org/10.1016/J.APENERGY.2018.04.111>.
- 627 [2] Logan BE, Elimelech M. Membrane-based processes for sustainable power  
628 generation using water. *Nature* 2012;488:313–9.  
629 <https://doi.org/10.1038/nature11477>.
- 630 [3] Van Vliet MTH, Wiberg D, Leduc S, Riahi K. Power-generation system  
631 vulnerability and adaptation to changes in climate and water resources. *Nat Clim*  
632 *Chang* 2016;6:375–80. <https://doi.org/10.1038/nclimate2903>.
- 633 [4] Adamovic M, Bisselink B, De Felice M, De Roo A, Dorati C, Ganora D, et al.  
634 Water – Energy Nexus in Europe. Luxembourg: Publications Office of the  
635 European Union; 2019. <https://doi.org/10.2760/968197>.
- 636 [5] Rani A, Snyder SW, Kim H, Lei Z, Pan SY. Pathways to a net-zero-carbon water  
637 sector through energy-extracting wastewater technologies. *Npj Clean Water* 2022  
638 51 2022;5:1–17. <https://doi.org/10.1038/s41545-022-00197-8>.

- 639 [6] IEA. WEO-2016 Special Report: Water-Energy Nexus. Paris: 2016.  
640 <https://doi.org/10.1021/es2016632>.
- 641 [7] van Vliet MTH, Jones ER, Flörke M, Franssen WHP, Hanasaki N, Wada Y, et al.  
642 Global water scarcity including surface water quality and expansions of clean  
643 water technologies. *Environ Res Lett* 2021;16:024020.  
644 <https://doi.org/10.1088/1748-9326/ABBFC3>.
- 645 [8] Voutchkov N. Energy use for membrane seawater desalination – current status and  
646 trends. *Desalination* 2018;431:2–14. <https://doi.org/10.1016/j.desal.2017.10.033>.
- 647 [9] Schunke AJ, Hernandez Herrera GA, Padhye L, Berry T-AA. Energy Recovery in  
648 SWRO Desalination: Current Status and New Possibilities. *Front Sustain Cities*  
649 2020;2:9. <https://doi.org/10.3389/FRSC.2020.00009>.
- 650 [10] Cornejo PK, Santana MVE, Hokanson DR, Mihelcic JR, Zhang Q. Carbon  
651 footprint of water reuse and desalination: a review of greenhouse gas emissions  
652 and estimation tools. *J Water Reuse Desalin* 2014;4:238–52.  
653 <https://doi.org/10.2166/WRD.2014.058>.
- 654 [11] Parkinson S. Guiding urban water management towards 1.5 °C. *Npj Clean Water*  
655 2021;4:1–6. <https://doi.org/10.1038/s41545-021-00126-1>.
- 656 [12] Alliance GCWD. Global Clean Water Desalination Alliance “H2O minus CO2.”  
657 2015.
- 658 [13] Eke J, Yusuf A, Giwa A, Sodiq A. The global status of desalination: An assessment  
659 of current desalination technologies, plants and capacity. *Desalination*  
660 2020;495:114633. <https://doi.org/10.1016/J.DESAL.2020.114633>.
- 661 [14] Jones E, Qadir M, van Vliet MTH, Smakhtin V, Kang S. The state of desalination  
662 and brine production: A global outlook. *Sci Total Environ* 2019;657:1343–56.  
663 <https://doi.org/10.1016/J.SCITOTENV.2018.12.076>.
- 664 [15] Pistocchi A, Bleninger T, Breyer C, Caldera U, Dorati C, Ganora D, et al. Can  
665 seawater desalination be a win-win fix to our water cycle? *Water Res*  
666 2020;182:115906. <https://doi.org/10.1016/J.WATRES.2020.115906>.
- 667 [16] Elimelech M, Phillip WA. The Future of Seawater Desalination: Energy,  
668 Technology, and the Environment. *Science* (80- ) 2011;333:712–7.  
669 <https://doi.org/10.1126/science.1200488>.
- 670 [17] Bundschuh J, Kaczmarczyk M, Ghaffour N, Tomaszewska B. State-of-the-art of  
671 renewable energy sources used in water desalination: Present and future prospects.  
672 *Desalination* 2021;508:115035. <https://doi.org/10.1016/J.DESAL.2021.115035>.
- 673 [18] Nam J-Y, Hwang K-S, Kim H-C, Jeong H, Kim H, Jwa E, et al. Assessing the  
674 behavior of the feed-water constituents of a pilot-scale 1000-cell-pair reverse  
675 electro dialysis with seawater and municipal wastewater effluent. *Water Res*  
676 2019;148:261–71. <https://doi.org/10.1016/J.WATRES.2018.10.054>.
- 677 [19] Tedesco M, Cipollina A, Tamburini A, Micale G. Towards 1 kW power production  
678 in a reverse electro dialysis pilot plant with saline waters and concentrated brines.  
679 *J Memb Sci* 2017;522:226–36. <https://doi.org/10.1016/j.memsci.2016.09.015>.

- 680 [20] Post JW, Goeting CH, Valk J, Goinga S, Veerman J, Hamelers HVM, et al.  
681 Towards implementation of reverse electrodialysis for power generation from  
682 salinity gradients. *Desalin Water Treat* 2010;16:182–93.  
683 <https://doi.org/10.5004/dwt.2010.1093>.
- 684 [21] Kempener R, Neumann F. *Salinity Gradient Energy Technology Brief*. IRENA  
685 *Ocean Energy Technol* 2014.
- 686 [22] Jang J, Kang Y, Han JH, Jang K, Kim CM, Kim IS. Developments and future  
687 prospects of reverse electrodialysis for salinity gradient power generation:  
688 Influence of ion exchange membranes and electrodes. *Desalination*  
689 2020;491:114540. <https://doi.org/10.1016/j.desal.2020.114540>.
- 690 [23] IRENA. *Innovation outlook: Ocean energy technologies*. 2020.
- 691 [24] Mehdizadeh S, Kakihana Y, Abo T, Yuan Q, Higa M. Power generation  
692 performance of a pilot-scale reverse electrodialysis using monovalent selective  
693 ion-exchange membranes. *Membranes (Basel)* 2021;11:27.  
694 <https://doi.org/10.3390/MEMBRANES11010027>.
- 695 [25] Pattle RE. Production of Electric Power by mixing Fresh and Salt Water in the  
696 Hydroelectric Pile. *Nature* 1954;174:660–660. <https://doi.org/10.1038/174660a0>.
- 697 [26] Chae S, Kim H, Gi Hong J, Jang J, Higa M, Pishnamazi M, et al. Clean power  
698 generation from salinity gradient using reverse electrodialysis technologies:  
699 Recent advances, bottlenecks, and future direction. *Chem Eng J* 2023;452:139482.  
700 <https://doi.org/10.1016/J.CEJ.2022.139482>.
- 701 [27] Nazif A, Karkhanечи H, Saljoughi E, Mousavi SM, Matsuyama H. Recent  
702 progress in membrane development, affecting parameters, and applications of  
703 reverse electrodialysis: A review. *J Water Process Eng* 2022;47:102706.  
704 <https://doi.org/10.1016/J.JWPE.2022.102706>.
- 705 [28] Li W, Krantz WB, Cornelissen ER, Post JW, Verliefde ARD, Tang CY. A novel  
706 hybrid process of reverse electrodialysis and reverse osmosis for low energy  
707 seawater desalination and brine management. *Appl Energy* 2013;104:592–602.  
708 <https://doi.org/10.1016/j.apenergy.2012.11.064>.
- 709 [29] Badruzzaman M, Voutchkov N, Weinrich L, Jacangelo JG. Selection of  
710 pretreatment technologies for seawater reverse osmosis plants: A review.  
711 *Desalination* 2019;449:78–91. <https://doi.org/10.1016/j.desal.2018.10.006>.
- 712 [30] Long R, Li B, Liu Z, Liu W. Reverse electrodialysis: modelling and performance  
713 analysis based on multi-objective optimization. *Energy* 2018;151:1–10.  
714 <https://doi.org/10.1016/j.energy.2018.03.003>.
- 715 [31] Long R, Li B, Liu Z, Liu W. Performance analysis of reverse electrodialysis stacks:  
716 Channel geometry and flow rate optimization. *Energy* 2018;158:427–36.  
717 <https://doi.org/10.1016/J.ENERGY.2018.06.067>.
- 718 [32] Ciofalo M, La Cerva M, Di Liberto M, Gurreri L, Cipollina A, Micale G.  
719 Optimization of net power density in Reverse Electrodialysis. *Energy*  
720 2019;181:576–88. <https://doi.org/10.1016/J.ENERGY.2019.05.183>.

- 721 [33] Altıok E, Kaya TZ, Othman NH, Kınalı O, Kitada S, Güler E, et al. Investigations  
722 on the effects of operational parameters in reverse electrodialysis system for  
723 salinity gradient power generation using central composite design (CCD).  
724 *Desalination* 2022;525:115508. <https://doi.org/10.1016/J.DESAL.2021.115508>.
- 725 [34] Faghihi P, Jalali A. An artificial neural network-based optimization of reverse  
726 electrodialysis power generating cells using CFD and genetic algorithm. *Int J*  
727 *Energy Res* 2022:1–17. <https://doi.org/10.1002/ER.8379>.
- 728 [35] Weiner AM, McGovern RK, Lienhard V JH. Increasing the power density and  
729 reducing the levelized cost of electricity of a reverse electrodialysis stack through  
730 blending. *Desalination* 2015;369:140–8.  
731 <https://doi.org/10.1016/j.desal.2015.04.031>.
- 732 [36] Papapetrou M, Kosmadakis G, Giacalone F, Ortega-Delgado B, Cipollina A,  
733 Tamburini A, et al. Evaluation of the Economic and Environmental Performance  
734 of Low-Temperature Heat to Power Conversion using a Reverse Electrodialysis –  
735 Multi-Effect Distillation System. *Energies* 2019;12:3206.  
736 <https://doi.org/10.3390/en12173206>.
- 737 [37] Giacalone F, Papapetrou M, Kosmadakis G, Tamburini A, Micale G, Cipollina A.  
738 Application of reverse electrodialysis to site-specific types of saline solutions: A  
739 techno-economic assessment. *Energy* 2019;181:532–47.  
740 <https://doi.org/10.1016/j.energy.2019.05.161>.
- 741 [38] Daniilidis A, Herber R, Vermaas DA. Upscale potential and financial feasibility of  
742 a reverse electrodialysis power plant. *Appl Energy* 2014;119:257–65.  
743 <https://doi.org/10.1016/j.apenergy.2013.12.066>.
- 744 [39] Yip NY, Brogioli D, Hamelers HVM, Nijmeijer K. Salinity gradients for  
745 sustainable energy: Primer, progress, and prospects. *Environ Sci Technol*  
746 2016;50:12072–94. <https://doi.org/10.1021/acs.est.6b03448>.
- 747 [40] Simões C, Pintossi D, Saakes M, Brillman W. Optimizing multistage reverse  
748 electrodialysis for enhanced energy recovery from river water and seawater:  
749 Experimental and modeling investigation. *Adv Appl Energy* 2021;2:100023.  
750 <https://doi.org/10.1016/J.ADAPEN.2021.100023>.
- 751 [41] Hu J, Xu S, Wu X, Wu D, Jin D, Wang P, et al. Multi-stage reverse electrodialysis:  
752 Strategies to harvest salinity gradient energy. *Energy Convers Manag*  
753 2019;183:803–15. <https://doi.org/10.1016/J.ENCONMAN.2018.11.032>.
- 754 [42] Hu J, Xu S, Wu X, Wang S, Zhang X, Yang S, et al. Experimental investigation  
755 on the performance of series control multi-stage reverse electrodialysis. *Energy*  
756 *Convers Manag* 2020;204:112284.  
757 <https://doi.org/10.1016/J.ENCONMAN.2019.112284>.
- 758 [43] Veerman J. Reverse electrodialysis: Co-and counterflow optimization of  
759 multistage configurations for maximum energy efficiency. *Membranes (Basel)*  
760 2020;10:1–13. <https://doi.org/10.3390/membranes10090206>.
- 761 [44] Veerman J, Saakes M, Metz SJ, Harmsen GJ. Reverse electrodialysis: A validated  
762 process model for design and optimization. *Chem Eng J* 2011;166:256–68.

- 763 <https://doi.org/10.1016/j.cej.2010.10.071>.
- 764 [45] Vermaas DA, Veerman J, Yip NY, Elimelech M, Saakes M, Nijmeijer K. High  
765 efficiency in energy generation from salinity gradients with reverse electrodialysis.  
766 ACS Sustain Chem Eng 2013;1:1295–302. <https://doi.org/10.1021/sc400150w>.
- 767 [46] Simões C, Pintossi D, Saakes M, Borneman Z, Brilman W, Nijmeijer K. Electrode  
768 segmentation in reverse electrodialysis: Improved power and energy efficiency.  
769 Desalination 2020;492:114604. <https://doi.org/10.1016/j.desal.2020.114604>.
- 770 [47] Pintossi D, Simões C, Saakes M, Borneman Z, Nijmeijer K. Predicting reverse  
771 electrodialysis performance in the presence of divalent ions for renewable energy  
772 generation. Energy Convers Manag 2021;243:114369.  
773 <https://doi.org/10.1016/J.ENCONMAN.2021.114369>.
- 774 [48] Simões C, Vital B, Sleutels T, Saakes M, Brilman W. Scaled-up multistage reverse  
775 electrodialysis pilot study with natural waters. Chem Eng J 2022;450:138412.  
776 <https://doi.org/10.1016/J.CEJ.2022.138412>.
- 777 [49] Doornbusch GJ, Bel M, Tedesco M, Post JW, Borneman Z, Nijmeijer K. Effect of  
778 membrane area and membrane properties in multistage electrodialysis on seawater  
779 desalination performance. J Memb Sci 2020;611:118303.  
780 <https://doi.org/10.1016/j.memsci.2020.118303>.
- 781 [50] Veerman J, Saakes M, Metz SJ, Harmsen GJ. Reverse electrodialysis: Performance  
782 of a stack with 50 cells on the mixing of sea and river water. J Memb Sci  
783 2009;327:136–44. <https://doi.org/10.1016/j.memsci.2008.11.015>.
- 784 [51] Tedesco M, Mazzola P, Tamburini A, Micale G, Bogle IDL, Papapetrou M, et al.  
785 Analysis and simulation of scale-up potentials in reverse electrodialysis. Desalin  
786 Water Treat 2015;55:3391–403. <https://doi.org/10.1080/19443994.2014.947781>.
- 787 [52] Grossmann IE, Caballero JA, Yeomans H. Mathematical programming approaches  
788 to the synthesis of chemical process systems. Korean J Chem Eng 1999 164  
789 1999;16:407–26. <https://doi.org/10.1007/BF02698263>.
- 790 [53] Guillén-Gosálbez G, You F, Galán-Martín Á, Pozo C, Grossmann IE. Process  
791 systems engineering thinking and tools applied to sustainability problems: current  
792 landscape and future opportunities. Curr Opin Chem Eng 2019;26:170–9.  
793 <https://doi.org/10.1016/j.coche.2019.11.002>.
- 794 [54] Grossmann IE, Trespalacios F. Systematic modeling of discrete-continuous  
795 optimization models through generalized disjunctive programming. AIChE J  
796 2013;59:3276–95. <https://doi.org/10.1002/aic.14088>.
- 797 [55] Tristán C, Fallanza M, Ibáñez R, Ortiz I, Grossmann IE. A generalized disjunctive  
798 programming model for the optimal design of reverse electrodialysis process for  
799 salinity gradient-based power generation. Comput Chem Eng 2023:108196.  
800 <https://doi.org/https://doi.org/10.1016/j.compchemeng.2023.108196>.
- 801 [56] Tristán C, Fallanza M, Ibáñez R, Ortiz I. Recovery of salinity gradient energy in  
802 desalination plants by reverse electrodialysis. Desalination 2020;496:114699.  
803 <https://doi.org/10.1016/j.desal.2020.114699>.

- 804 [57] Ortiz-Imedio R, Gomez-Coma L, Fallanza M, Ortiz A, Ibañez R, Ortiz I.  
805 Comparative performance of Salinity Gradient Power-Reverse Electrodialysis  
806 under different operating conditions. *Desalination* 2019;457:8–21.  
807 <https://doi.org/10.1016/J.DESAL.2019.01.005>.
- 808 [58] Chen Q, Grossmann IE. Recent Developments and Challenges in Optimization-  
809 Based Process Synthesis. <https://doi.org/10.1146/Annurev-Chembioeng-080615-033546>  
810 2017;8:249–83. <https://doi.org/10.1146/ANNUREV-CHEMBIOENG-080615-033546>.  
811
- 812 [59] EUROSTAT. Electricity prices for non-household consumers - bi-annual data  
813 (from 2007 onwards) [NRG\_PC\_205] n.d.  
814 <https://ec.europa.eu/eurostat/databrowser/bookmark/65f83096-1534-4ddc-a561-44764c07601c?lang=en> (accessed April 3, 2023).  
815
- 816 [60] ICAP. Allowance Price Explorer 2022. <https://icapcarbonaction.com/en/ets-prices>  
817 (accessed May 8, 2023).
- 818 [61] Hart WE, Laird CD, Watson J-P, Woodruff DL, Hackebeitl GA, Nicholson BL, et  
819 al. *Pyomo — Optimization Modeling in Python*. vol. 67. Second Edi. Cham:  
820 Springer International Publishing; 2017. <https://doi.org/10.1007/978-3-319-58821-6>.  
821
- 822 [62] Chen Q, Johnson ES, Bernal DE, Valentin R, Kale S, Bates J, et al. *Pyomo.GDP:*  
823 *an ecosystem for logic based modeling and optimization development*. *Optim Eng*  
824 2021:1–36. <https://doi.org/10.1007/s11081-021-09601-7>.
- 825 [63] Lee S, Grossmann IE. A global optimization algorithm for nonconvex generalized  
826 disjunctive programming and applications to process systems. *Comput Chem Eng*  
827 2001;25:1675–97. [https://doi.org/10.1016/S0098-1354\(01\)00732-3](https://doi.org/10.1016/S0098-1354(01)00732-3).
- 828 [64] Chen Q, Johnson ES, Sirola JD, Grossmann IE. *Pyomo.GDP: Disjunctive Models*  
829 *in Python*. *Comput. Aided Chem. Eng.*, vol. 44, Elsevier B.V.; 2018, p. 889–94.  
830 <https://doi.org/10.1016/B978-0-444-64241-7.50143-9>.
- 831 [65] Forgacs C. Recent developments in the utilization of salinity power. *Desalination*  
832 1982;40:191–5. [https://doi.org/10.1016/S0011-9164\(00\)88683-X](https://doi.org/10.1016/S0011-9164(00)88683-X).
- 833 [66] Meyer-Steele S, von Gottberg A, Talavera JL. New Sea Water Reverse Osmosis  
834 Plant for the Carribean “Energy Recovery, Brine Recovery & Cost Reduction.”  
835 2001.
- 836 [67] Portillo E, de la Rosa MR, Louzara G, Quesada J, Ruiz JM, Mendoza H. Dispersion  
837 of desalination plant brine discharge under varied hydrodynamic conditions in the  
838 south of Gran Canaria. *Desalin Water Treat* 2014;52:164–77.  
839 <https://doi.org/10.1080/19443994.2013.795349>.
- 840 [68] Sadhwani Alonso JJ, Melián-Martel N. Environmental Regulations—Inland and  
841 Coastal Desalination Case Studies. In: Gude VG, editor. *Sustain. Desalin. Handb.*  
842 *Plant Sel. Des. Implement.*, Butterworth-Heinemann; 2018, p. 403–35.  
843 <https://doi.org/10.1016/B978-0-12-809240-8.00010-1>.
- 844 [69] Pérez Talavera J, Quesada Ruiz J. Identification of the mixing processes in brine  
845 discharges carried out in Barranco del Toro Beach, south of Gran Canaria (Canary



- 846 Islands). *Desalination* 2001;139:277–86. <https://doi.org/10.1016/S0011->  
847 9164(01)00320-4.
- 848 [70] OECD. *Effective Carbon Rates 2021: Pricing Carbon Emissions through Taxes*  
849 *and Emissions Trading*. Paris: OECD; 2021. <https://doi.org/10.1787/0e8e24f5-en>.
- 850 [71] Small Business Innovation Research (SBIR) and Small Business Technology  
851 Transfer (STTR) programs. *Low-Cost Manufacturing of High-Performance Ion*  
852 *Exchange Membranes for Electrodialysis using Initiated Chemical Vapor*  
853 *Deposition* n.d. <https://www.sbir.gov/node/2282063> (accessed December 8, 2022).
- 854 [72] IRENA. *Renewable Power Generation Costs in 2021*. Abu Dhabi: 2021.
- 855 [73] Turek M, Bandura B. *Renewable energy by reverse electrodialysis*. *Desalination*  
856 2007;205:67–74. <https://doi.org/10.1016/J.DESAL.2006.04.041>.
- 857 [74] Turek M, Bandura B, Dydo P. *Power production from coal-mine brine utilizing*  
858 *reversed electrodialysis*. *Desalination* 2008;221:462–6.  
859 <https://doi.org/10.1016/J.DESAL.2007.01.106>.
- 860 [75] Weiner AM, McGovern RK, Lienhard V JH. *A new reverse electrodialysis design*  
861 *strategy which significantly reduces the levelized cost of electricity*. *J Memb Sci*  
862 2015;493:605–14. <https://doi.org/10.1016/j.memsci.2015.05.058>.
- 863 [76] Bevacqua M, Tamburini A, Papapetrou M, Cipollina A, Micale G, Piacentino A.  
864 *Reverse electrodialysis with NH<sub>4</sub>HCO<sub>3</sub>-water systems for heat-to-power*  
865 *conversion*. *Energy* 2017;137:1293–307.  
866 <https://doi.org/10.1016/J.ENERGY.2017.07.012>.
- 867 [77] Micari M, Cipollina A, Giacalone F, Kosmadakis G, Papapetrou M, Zaragoza G,  
868 et al. *Towards the first proof of the concept of a Reverse ElectroDialysis -*  
869 *Membrane Distillation Heat Engine*. *Desalination* 2019;453:77–88.  
870 <https://doi.org/10.1016/j.desal.2018.11.022>.
- 871 [78] Ranade A, Singh K, Tamburini A, Micale G, Vermaas DA. *Feasibility of*  
872 *Producing Electricity, Hydrogen, and Chlorine via Reverse Electrodialysis*.  
873 *Environ Sci Technol* 2022;2022:16062–72.  
874 <https://doi.org/10.1021/ACS.EST.2C03407/ASSET/IMAGES/LARGE/ES2C034>  
875 07\_0007.JPEG.
- 876 [79] Roald LA, Pozo D, Papavasiliou A, Molzahn DK, Kazempour J, Conejo A. *Power*  
877 *systems optimization under uncertainty: A review of methods and applications*.  
878 *Electr Power Syst Res* 2023;214:108725.  
879 <https://doi.org/10.1016/J.EPSR.2022.108725>.

880